Investigation Of Alternating Bands In Friction Stir Welds Of Aluminum Alloys

Balamurugan Balakrishnan[1] , Ramarao Mathialagan[2*], Vijayaram Raghavan Thoguluva[3] , Ramamurthy Annamalai[4]

[1]Research Scholar, Department of Mechanical Engineering, Bharath Institute of Higher Education and Research, Chennai, -600073 Tamil Nadu, India.
[2,4] AssociateProfessor,Department of Mechanical Engineering, Bharath Institute of Higher Education and Research, Chennai,- 600073 Tamil Nadu, India.
[3]Professor, Department of Mechanical Engineering, Bharath Institute of Higher Education and Research, Chennai, - 600073 Tamil Nadu, India.
Corresponding author: ramarao.mech@bharathuniv.ac.in

ABSTRACT:

Friction stir welding (FSW) is a solid-state welding process that involves complex phenomena influenced by welding parameters such as feed and rotation speeds, as well as the tool geometry. These parameters condition the temperature cycles, which in turn affect the microstructure and mechanical properties of the weld. This study investigates the formation of alternating bands in FSW aluminium alloys, specifically focusing on the impact of welding parameters, tool geometry, and grain boundary characteristics. The alternating bands are identified as regions of contrasting grain structures, with differences observed in grain size and boundary orientation. High-angle (HA) boundaries, predominantly (111), and low-angle (LA) boundaries, predominantly (101), are found to alternate within the bands. Hardness tests, including Vickers and nano-indentation, show no significant variation in hardness between the alternating bands. The weld core consists of larger grains with HA joints and smaller grains with LA joints. The RS, on the other hand, contains equiaxed grains with HA joints and random orientations. Furthermore, the microstructure formed by HA grain boundaries exhibits a higher concentration of particles compared to the LA boundary areas. These findings provide new insights into the relationship between welding parameters, microstructure, and mechanical properties in friction stir welds.

Keywords: Friction stir welding, alternating bands, grain boundaries, tool geometry, welding parameters, microstructure, mechanical properties, Vickers hardness, nano-indentation, aluminum alloys.

1. INTRODUCTION:

Since the invention of the friction stir welding (FSW) process by The Welding Institute (TWI) in 1991, extensive research has been conducted to understand the effects of process parameters on the microstructural, thermal, and mechanical properties (MP) of joints, with the aim of optimizing weld quality [1-6]. The microstructure of a friction stir weld (FSW) differs significantly from that of traditional fusion welds, such as arc welding (MIG and MAG). While fusion welds are characterized by a molten metal core, a heat-affected zone, and base metal, FSWs feature distinct zones: the weld core (where the metal remains below melting temperature), a thermo-mechanically affected zone, a heat-affected zone, and base metal [4-8]. The weld core is known to contain very fine, equiaxed grains that measure only a few micrometers, often resulting from dynamic recrystallization (Su, Wu, and Huang 2019). One notable structural feature in FSWs is the formation of alternating bands, commonly referred to as “onion rings,” which are visible under optical microscopy as concentric circles in the transverse section of the weld [5-10].

The phenomenon of onion ring formation was initially explained by [2], who proposed that it results from the interaction of tool rotation and advancement. Subsequent studies, such as those by [3] and [1], have offered different interpretations, with some attributing the band alternation to variations in both grain size and precipitate concentration, while others attribute it solely to precipitate concentration differences. These discrepancies highlight the complex and unique nature of each weld, underscoring the ongoing need for research to fully characterize each zone within FSWs [11-13].

Understanding the microstructural characteristics of these alternating bands is crucial for improving the MP of FSWs. This study aims to investigate the alternating bands in the weld core of aluminum joints and assess their impact on mechanical performance. To accomplish this, welds will be produced using various process parameters (rotation speed (RS), FR, and tool type) on two 6000-series aluminum alloys (AAs): 6061-T651 and 6082-T6 [13-15]. Detailed microstructural analysis, including grain size and hardness measurements, will be conducted on these bands. Additionally, a sample displaying an extensive area of alternating bands on one side of the weld will be selected for comparative analysis with the side that lacks these bands [16-17]. An Electron Backscatter Diffraction (EBSD) analysis will further examine grain orientation and misorientation within these bands and other weld zones, enhancing our understanding of how these unique microstructural features influence overall weld integrity and strength.

2. LITERATURE REVIEW:

This study [18] provides a comprehensive review of FSW's advancements in joining AAs, discussing process parameters such as tool RS, FR, and tool geometry. It focuses on how these parameters affect the microstructural zones within the weld, including the weld nugget, thermo-mechanically affected zone (TMAZ), and heat-affected zone (HAZ). Key findings suggest that optimal parameter control can significantly enhance grain refinement and, thus, the MP of aluminum joints, notably their tensile strength and hardness.

This research [19] investigates the microstructural evolution of friction stir-welded 6061-T6 aluminum, examining how different welding parameters (WP) influence grain size and MP. The study reveals that increasing tool RS promotes finer equiaxed grains due to dynamic recrystallization, improving hardness and tensile strength. Furthermore, it shows that higher FRs result in wider heat-affected zones, impacting overall weld quality.

This study [20] examines the effect of FSW parameters on microstructural and MP of 7075 AA joints. Through microstructural analysis, it identifies how different cooling rates in the weld zones influence grain structure, precipitate formation, and overall mechanical performance. It concludes that optimized rotational speeds (RSs) and feed rates (FRs) can mitigate thermal gradients, resulting in superior strength and hardness.

This research [21] focuses on the formation of grain boundary bands, often referred to as "onion rings," in friction stir-welded aluminum joints. Through an analysis of the welding process and tool geometry, it explores how these alternating bands impact weld strength. The findings suggest that careful tuning of tool geometry and RSs minimizes defects within the weld, producing highly refined grains with improved MP such as increased yield strength and fatigue resistance.

This study [22] addresses grain refinement mechanisms in FSW of 6082-T6 AA. Using electron backscatter diffraction (EBSD) analysis, it provides a detailed examination of dynamic recrystallization processes within the weld zone. The study concludes that tool RS and plunge depth are critical for controlling grain size and orientation, with optimized parameters yielding ultrafine grains that enhance the weld’s hardness and strength.

This updated study [23] from leading FSW researchers delves into recent developments in FSW for high-strength AAs, specifically discussing advancements in tool design and process parameters for improved grain refinement. The review emphasizes the effects of pin profiles on the grain structure in different microstructural zones and provides recommendations for tool design that optimize MP. The researchers suggest that proper tool and parameter selection can achieve superior weld integrity in challenging AAs.

This work [24] studies the effect of cooling media on the microstructure and MP of friction stir-welded 6061-T6 AA. By using different cooling conditions such as water and air, the study examines how cooling rate affects microstructural characteristics and weld performance. Findings reveal that water-cooled welds achieve finer grains with higher hardness, while air-cooled welds offer more ductility, indicating the potential to customize FSW joint properties through controlled cooling.

This recent study [25] explores the use of hybrid FSW with advanced tool materials, focusing on wear resistance and tool life during AA welding. The research details how new tungsten carbide-based tools withstand high temperatures and maintain structural integrity, enabling deeper weld penetration and superior grain refinement. The study highlights improvements in joint strength and hardness, attributed to the tool's ability to sustain consistent frictional heat.

3. Experimental Approach:

In this work, we focused on AAs, particularly 6061-T651 and 6082-T6, which belong to the 6000 series where silicon and magnesium are the primary alloying elements. For welding, 6061-T651 AA rolled bars, 4 mm thick, were cut into 30 mm long pieces, while 6082-T6 alloy plates, 6 mm thick, were also cut into 30 mm long sections. The welds were oriented along the rolling direction. These alloys were chosen for their excellent corrosion resistance, attributed to their low copper content, which helps to reduce additional defects. Commonly used in structural components for transportation and structural panels, these alloys are suited for applications requiring welding. FSW offers an alternative method to enhance their quality and reduce the structure's overall mass. The chemical compositions of 6061 and 6082 alloys are presented in Fig 1.

Alloy	Al	Si	Fe	Cu	Mn	Mg	Cr	Zn	Ti
6082	Balance	0.7 to 1.3	0.5	0.1	0.4 to 1	0.6 to 1.2	0.25	0.2	0.1
6061	Balance	0.69	0.33	0.26	0.08	0.97	0.08	0.02	0.02

Figure 1. Chemical Composition of 6061 and 6082 AAs (wt%)

The FSW machine at the Indian Institute of Technology (IIT) Madras was used for this study, equipped with a tool holder and a support mechanism for securely fastening the workpieces. WP, including rotation and feed speeds, were precisely controlled by the machine's numerical system, which enabled accurate positioning along the x, y, and z axes. The depth of tool immersion was also regulated on the z-axis, ensuring consistency and precision throughout the welding process.

The tests conducted were split into two parts: FSW of plates and other plates where the tool was rotated without a joint. This approach focused on the formation of alternating bands and eliminated defects related to poor fixation or oxide layers. Key WP included tool geometry and the tool's feed and RSs. Most tests used a conical tool with a 15.87 mm shoulder diameter and a 5 mm to 1.77 mm tapered pin, with a height of 2.8 mm. Additional samples produced at the Indian Institute of Technology (IIT) Madras involved a tool with a 12 mm shoulder diameter and a trigonal pin. Both tools were manufactured from tungsten carbide, chosen for its high strength and durability in handling high-temperature processing conditions.

Various feed and RSs, outlined in Table 1, were tested with the aim of forming alternating bands. For the first four tests, parameter values were taken from the literature on 6000 series alloys, ensuring consistency with prior studies. Further tests were conducted with a fixed feed speed of 100 mm/min and RSs of 800 and 1600 rpm. Samples from Pune, Maharashtra, India employed parameters specifically chosen to optimize banded structure formation, based on expert guidance tailored to local research conditions. The parameters were selected to enhance the formation of alternating bands in the alloy structure, aligning with findings from prior studies focused on 6000 series' AAs.

Table 1. Parameters Used in Testing in This Study

Sample code	Alloy	Tool	RS (rpm)	FR (mm/min)	RS/FR ratio
11SS1	6061-T651	Tapered	400	120	3.33
22SS1			900	300	3
33SS1			2000	40	50
44SS1			1120	160	7
82-1SS1	6082-T6		1600	100	16
82-2SS1			800	100	8
82-3SS1			1750	200	8.75
015		Trigonal	1500	400	3.75
016			1750	200	8.75
019			1500	300	5
020			2000	600	3.33

Upon visual inspection, plates treated with the conical tool exhibited flashes on the retreating side (RS), attributed to a large tool plunge depth or excessive heat input when the feed-to-RS ratio was high. Channels formed at the weld start and created vacuum defects on the advancing side (AS). While these defects did not affect the study's focus on strip structures, the weld's beginning and end were excluded from analysis to avoid insufficiently mixed material. Surface inspection revealed semicircles correlating with the feed and RSs, disappearing at higher RSs, leading to a sandblasted surface indicative of "surface galling" due to high heat input, potentially affecting weld MP.

Samples for metallography were prepared by cutting transverse weld sections, avoiding irregular weld start and end areas. They were polished according to a protocol in Table 2, using a sequence of silicon carbide abrasive papers and diamond suspension, then finished with a vibration polisher for optimal surface quality. Chemical etching trials identified Barker’s and Weck’s etchants as effective for revealing the microstructure of the kneaded zone.

Table 2. Polishing procedure

Grit polishing	240	600	800	1200	-	-
Time (min)	5	5	5	5	3	3
Lubricant/ Abrasive paper	water/ silicon carbide				Diamond suspension solution (1µ) / felt	Colloidal silica solution (0.05 µ) / felt

For scanning electron microscopy, EBSD analysis on Sample 016 used a Hitachi SU-8230 FE-SEM to examine grain orientation in alternating layers. This sample, welded with the trigonal tool at 1750 rpm and a 200 mm/min FR, exhibited broad alternating bands on the AS, contrasting with the RS.

Microhardness tests used a Vickers machine with a 10 g load, measuring indentations on areas containing alternating bands to assess hardness in light and dark bands. Nano-indentation targeted thinner bands and precipitate visualization with a diamond indenter in the Hitachi SU-8230 FE-SEM, using 50 mN force and timed loading and unloading for precise measurements.

4. Results and Discussion:

4.1 Microstructure observations

4.1.1 Optical microscopy of a weld

The band structure is visible even if the chemical etching does not reveal the grains. At first glance, the AS of the weld and the RS of the weld are clearly observed. On the AS, the boundary between the weld core and the heat-affected zone is very visible, while on the RS, it is rather blurred. An alternation between dark and light bands is also distinguished. Figure 2 shows a cross-section (c-s) of the weld that highlights these differences between the AS and RSs as well as the alternating bands near a cavity. Figure 3 (a) shows the alternating bands. In several samples, bands with grains with visible joints were observed and other bands where the grains could not be observed as shown in Figure 3 (b).

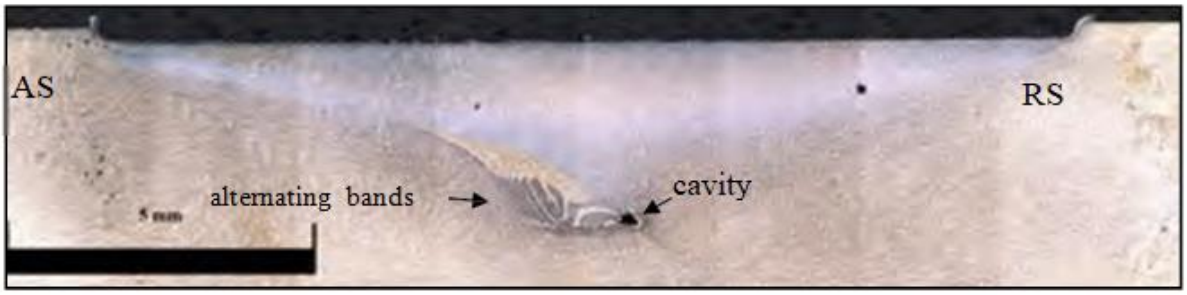

Figure 2. Optical microscopy of a c-s of a weld showing the stirred zone containing the alternating bands

Figure 3 (a) Optical microscopy of the banded structure and (b) zoom on some alternating bands

4.1.2 Location of the alternating bands in the microstructure

For all samples obtained by the friction stir process (FSP), the banded structure zone is formed in the AS. The bands are very close to each other near the boundary of the HAZ and the distance between them increases as they approach the core of the weld as can be seen in Figures 1 and 2. A void defect was observed for all samples made with the conical tool. This void persists throughout the weld, it is therefore a tunnel. The samples welded with the trigonal tool show alternating bands in the form of circles that

look more like "onion rings" spread over the entire bottom of the weld (on both sides AS and RS as shown in Figure 4 except for sample 016, which shows a similar banded structure to that of the samples made with the conical tool. This sample will be studied in more detail in the following paragraphs.

Figure 4. c-s of a weld with alternating bands distributed over the entire bottom

4.1.3 Grain size of the alternating bands

The weld core is characterized by very fine equiaxed grains. However, their size varies according to their position in the weld, as explained in the literature review. What was noticed in the optical microscope images of some samples where the chemical etching revealed the grains of all the bands, is that there is also a difference in the grain size between the bands "light" and "dark" bands located in the AS, but also between the zone of the banded structure and the receding side. Figure 5 (a) shows an enlarged area of the alternating bands separated by red lines, the middle one is the "dark" band with smaller grains and we have the "light" bands at both ends with larger grains. The receding side is shown in Figure 5 (b) and we can visually see that the grains are larger than those of the banded structure.

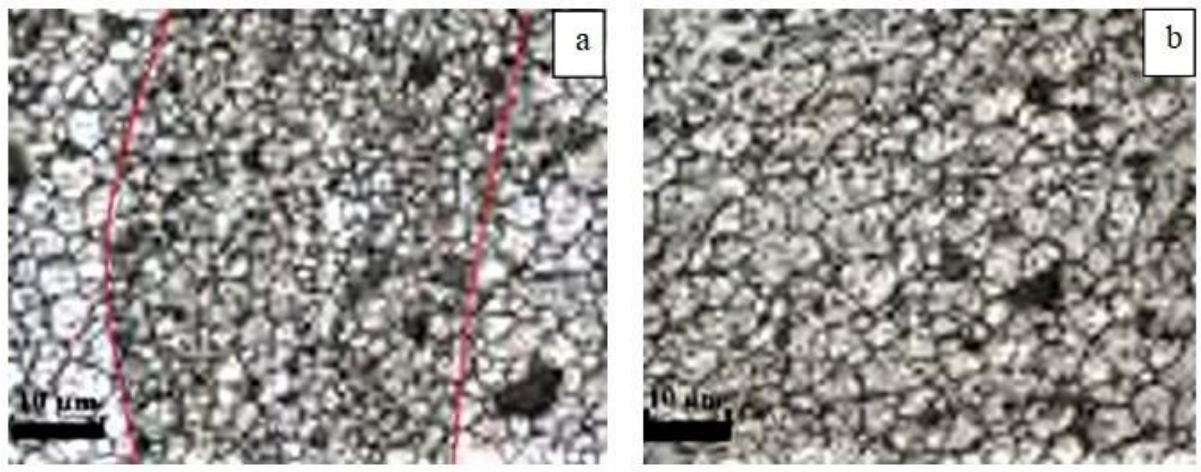

Figure 5. Optical micrograph of the weld core of sample 016: (a) the alternating bands and (b) the receding side

By measuring the grain size in the different alternating bands, we notice that the average diameter can vary from 3 to 7 µm. The curve in Figure 6 shows the variation in the average grain diameter of the different successive bands. However, the alternation between the bands with coarse grains and finer grains is not very visible. Indeed, the same band can contain grains of different sizes and the average value of their diameters gives us an erroneous estimate. Consequently, we calculated the percentages of

grains whose diameter, noted d, is < 3 µm, those whose diameter is between 6 and 10 µm and those whose diameter is greater than 10 µm. The curve in Figure 7 shows the variation in the percentage of these different grains. For example, band #3 consists of large grains with 33.2% of grains with a diameter greater than 6 µm and 15% greater than 10 µm, of which 8% is greater than 16 µm compared to only 29% of grains with a diameter < 3 µm. Band #8 consists of 64% of grains with a diameter < 3 µm compared to only 4% greater than 6 µm and not exceeding a maximum diameter of 7.5 µm.

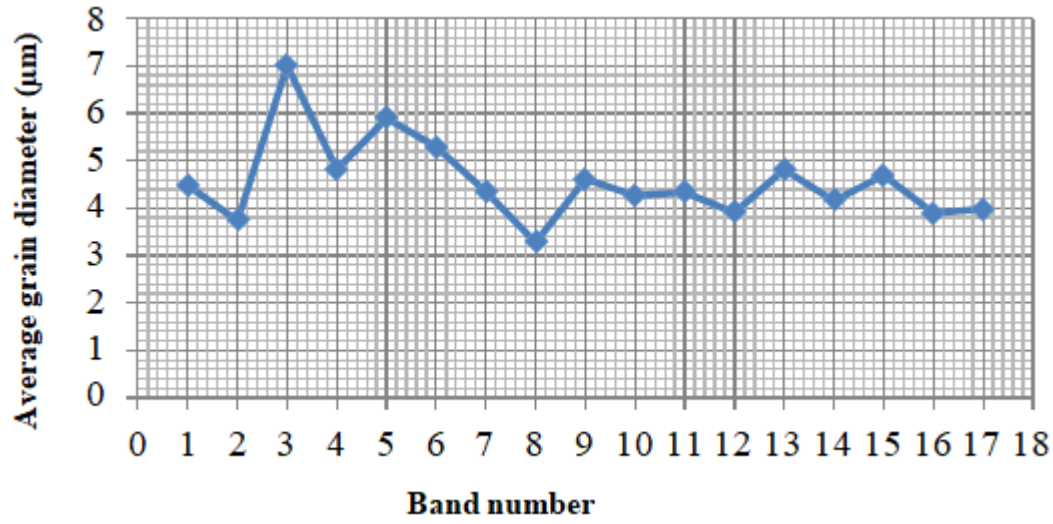

Figure 6. Average grain diameter in alternating bands

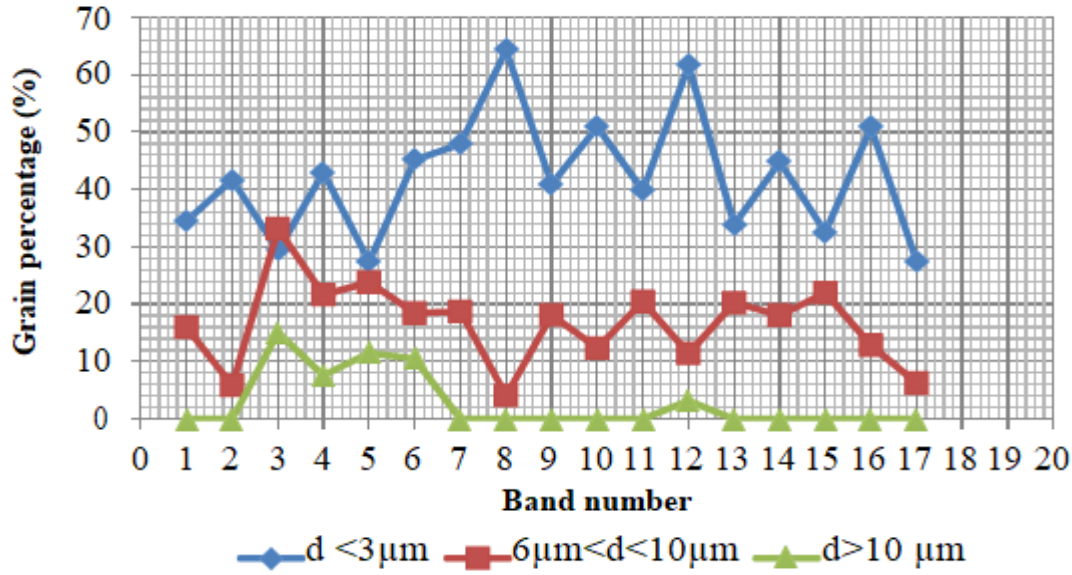

Figure 7. Percentage of grains with a diameter <3 µm, between 6 and 10 µm and >10 µm

Several researchers have studied the characteristics of alternating bands, a difference in grain size between these bands has not always been observed. They found a homogeneous grain size which they averaged for the entire weld core. In their study on 7039 AA, Sharma et al. compared the average grain size in the core as well as in the heat and thermomechanically affected zones by varying the feed and RSs. They found alternating bands in their microstructure and explained that they appeared when the heat input was not too high and that they decreased or disappeared at high RSs with an increase in grain size from 7.93 µm to 13.12 µm by increasing the RS from 410 rpm to 635 rpm [16]. Shneider and Nunes in their research on "onion rings" explained their origin by showing a difference in orientation and texture between the bands, without discussing the grain size [17]. Some researchers have noticed this difference in grain size between the bands of the "onion rings" like Mahoney et al.. In their analysis of a weld in alloy 7075-T651, they classified these bands into bands with fine grains between 5 and 10 µm

and bands with finer grains between 3 and 5 µm. The same trends were found with even finer grains, but what differs in our study compared to that of Mahoney et al. is that these values are not the averages of grain sizes but percentages. Indeed, there are bands containing many more very fine grains smaller than 3 µm (about 50% and exceeding 60% in some bands) and others with about 50% of grains larger than 6 µm.

In the following, we will try to understand the effect of this difference in grain size on the hardness of the alternating bands, in a first step, through a micro-hardness test and then by nano-indentation.

3.2 Influence of WP on the hardness of the alternating bands:

The base alloys 6061-T651 and 6082-T6 have the respective average hardness values of 113 and 116 HV. Only three samples will be analyzed, because the indentations coincide with the different alternating "light" and "dark" bands. The black dots in Figure 8 are the imprints left by the pyramid-shaped indenter.

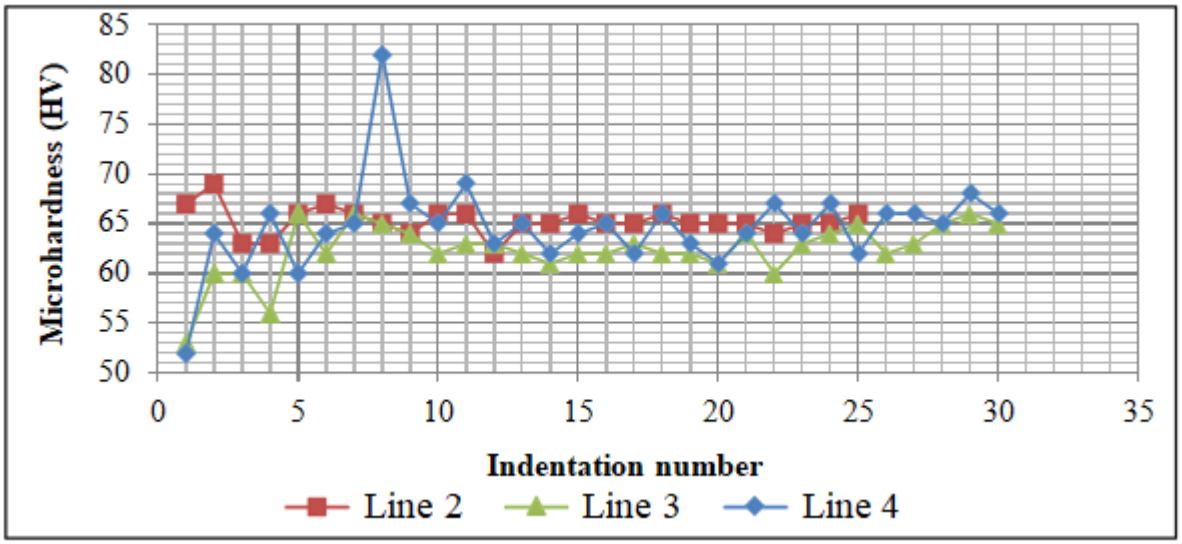

Figure 8. Microhardness profile of the alternating bands area

The study of Sutton et al. had shown a difference in hardness between the alternating bands of the longitudinal plane of a weld in alloy 2024-T3 (i.e. the semi-circular traces left by the tool) with bands of an average hardness of 132 HK and others of 139 HK [18]. However, in our study, all the hardness measurements carried out do not allow us to conclude that there is a difference between the dark bands and the light bands. Indeed, there is no clear trend in the curves and the gap between the different values does not exceed 10 HV. On the other hand, the measurements showed that the average hardness value in the alternating stripe area increases from 64 HV to 74 HV by decreasing the RS from 1600 rpm to 800 rpm for the same FR of 100 mm/min as shown in Figure 9. This confirms that the MP improve by decreasing the heat input by increasing the FR and decreasing the RS, while keeping a RS capable of ensuring good mixing of the material [19]. Rajakumar et al. studied the effect of process parameters (feed and RSs, applied force, tool) on several welds of 7075-T6 alloy. They noticed that the microhardness increased from 185 to 203 HV by decreasing the RS from 1800 rpm to 1400 rpm [20]. A study conducted on an AA 6061-T651, Lim et al. saw the microhardness values increase by more than 10 HV by decreasing the RS from 2000 rpm to 1600 rpm for a fixed FR of 400 mm/min [19].

It goes without saying that in FSW, the choice of parameters ensuring good joint quality depends heavily on the alloy but also on the tool used. Whether the heat input is high, or not enough, also depends on the alloy and its constituents. An example is a research by Prisco et al. on 2139-T351 alloy where they found that for a FR of 155 mm/min, a RS of 900 rpm would be too high causing excess heat input leading to burrs in the weld [21]. While Rajakumar, found that for a RS of 900 rpm and a FR of 60 mm/min, the heat input was insufficient causing poor material mixing and tunneling defect [20]. He noted that the MP of the weld were optimal for a RS of 1400 rpm and beyond this speed the quality deteriorated.

Indeed, when the temperature reaches too high values, the cooling time increases causing the coarsening of grains and precipitates and thus decreasing the hardness and MP [20].

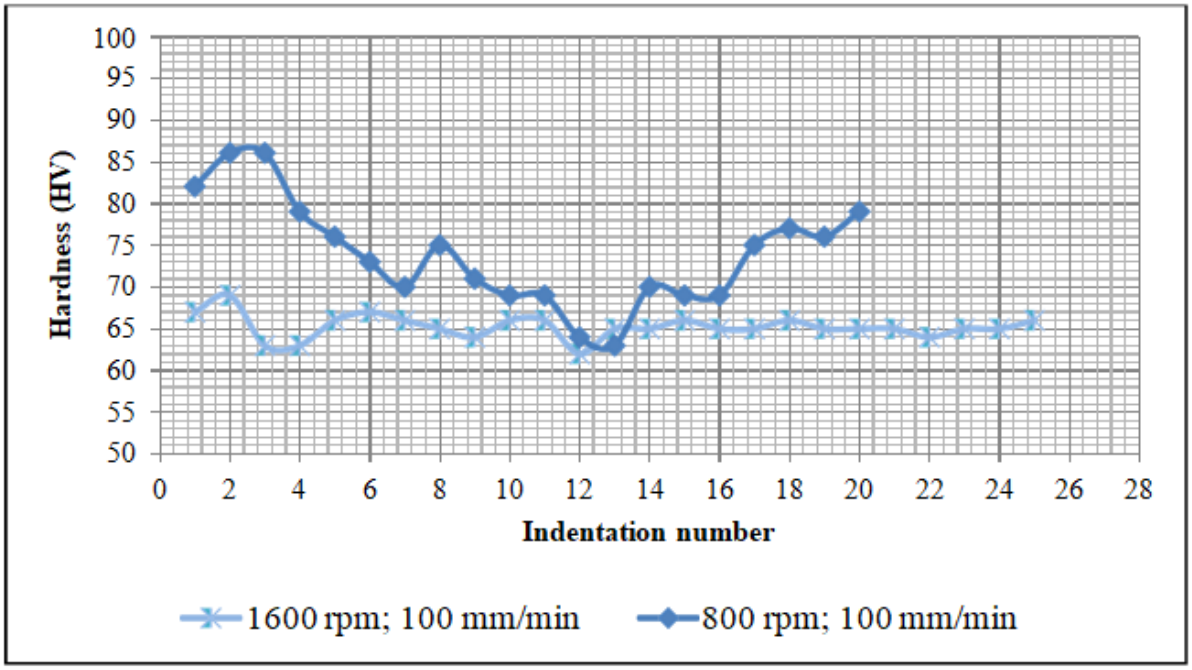

Figure 9. Hardness profile in the alternating band zone of two AA 6082-T6 welds as a function of the variation of the RS

4.3 Nano-indentation test:

Two lines of 15 indentations represented by the black spots in Figure 10 (b) were carried out to establish a hardness profile (Figure 10 (a)). Figure 10 (b) represents an inverse pole figure (IPF) mapping of the banded structure which shows an alternation between two different orientations (111) in blue and (101) in green. The highest value being 93 HV is found on a band whose grains have a (101) orientation (green band) and the lowest (65 HV) on a band whose grains have a (111) orientation (blue band). However, the nano-hardness profile does not correspond to an alternation of orientation between the bands.

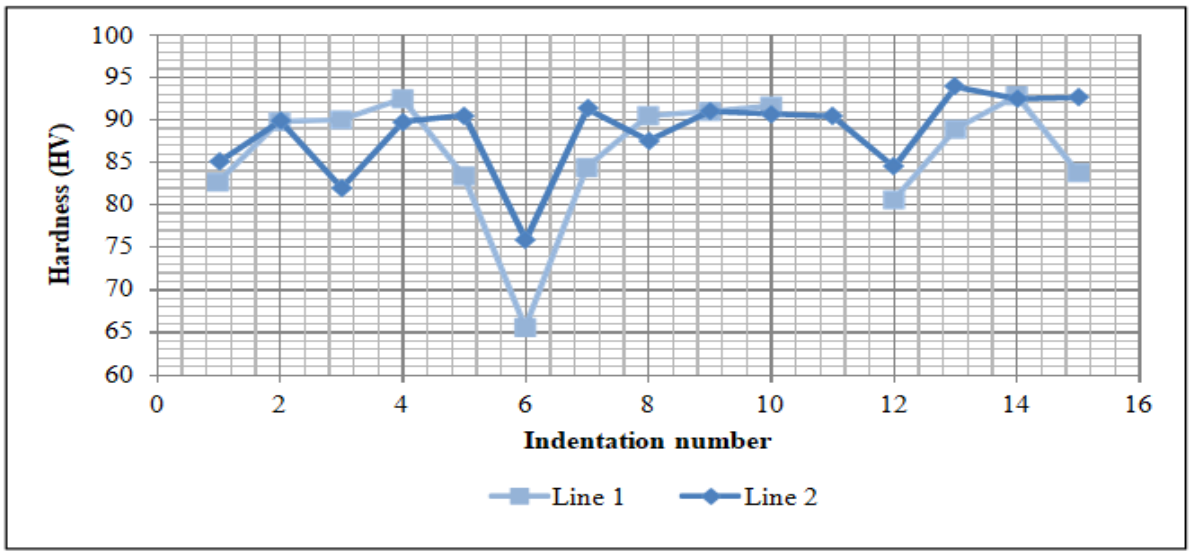

(a)

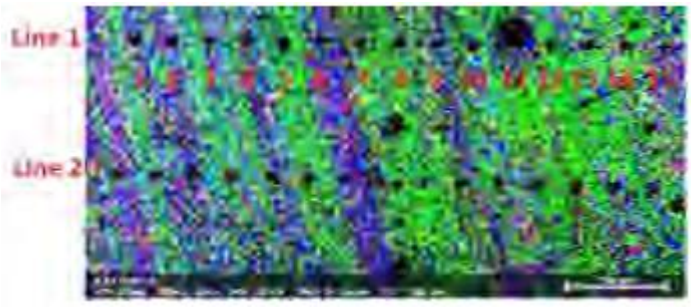

(b)

Figure 10 (a) Hardness profile measured by nano-indenters corresponding to the two measurement lines on the EBSD map in (b)

Of particular interest were points 5 and 6 of line 1 where a decrease in hardness was observed, confirmed by a second measurement on the same blue band of line 2 below. Points 14 and 15 will also be studied for the same reason. Figure 11 shows scanning electron microscope (SEM) images (left) and IPF maps (right) taken around these points. Indentation 5 is in a band with small grains and its hardness is higher than that of the band with larger grains where indentation 6 is located. While the opposite is true for points 14 and 15. Indentation 15 is in a band with small grains and its hardness is lower than that of the band with larger grains where indentation 14 is located. These observations show that the difference in hardness between the bands cannot be attributed solely to the grain size and that other factors must be considered such as the presence of precipitates.

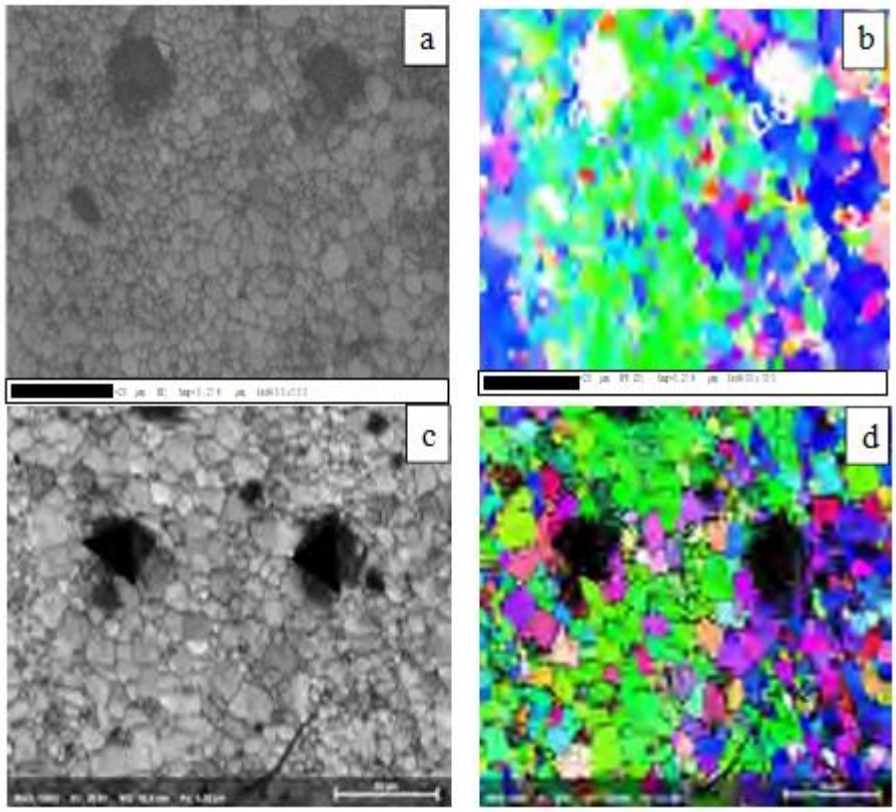

Figure 11 (a) SEM image of the area around indentations 5 and 6; (b) IPF mapping of the area around indentations 5 and 6; (c) SEM image of the area around indentations 14 and 15 and (d) IPF mapping of the area around indentations 14 and 15

4.4 Grain orientation and disorientation in FSWs

4.4.1 Grain orientation:

The simplified diagram in Figure 12 (a) shows the different zones of the weld (the nugget, the heat-affected zone HAZ and the base material MB) as well as the location of the zones to be studied relative to the AS and the RS. First, a low magnification image of the area to be studied was taken with a scanning electron microscope and which gives us an overall view of three zones as shown in Figure 12 (b) where zone 1 represents the heat affected zone, zone 2 represents the AS containing the alternating bands and the rest of the stirred zone (the center of the weld and the RS) is represented by zone 3. In this sample, the tunnel defect is found. The EBSD analysis was carried out on the four zones from I to IV shown in Figure 12. Zones II and III are located at the center of the weld on the tool path. Argus images of these four zones, obtained under backscattered electrons with the SEM, are presented in Appendix I. The EBSD mapping of the base alloy 6082 is shown in Figure 13 which shows a random orientation of the grains.

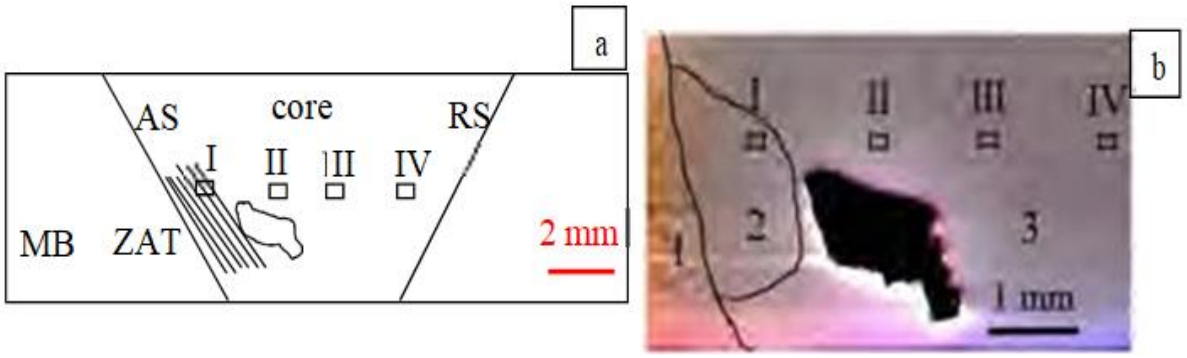

Figure 12. (a) Simplified diagram of the weld c-s and (b) SEM image showing the four areas analyzed by EBSD (I to IV)

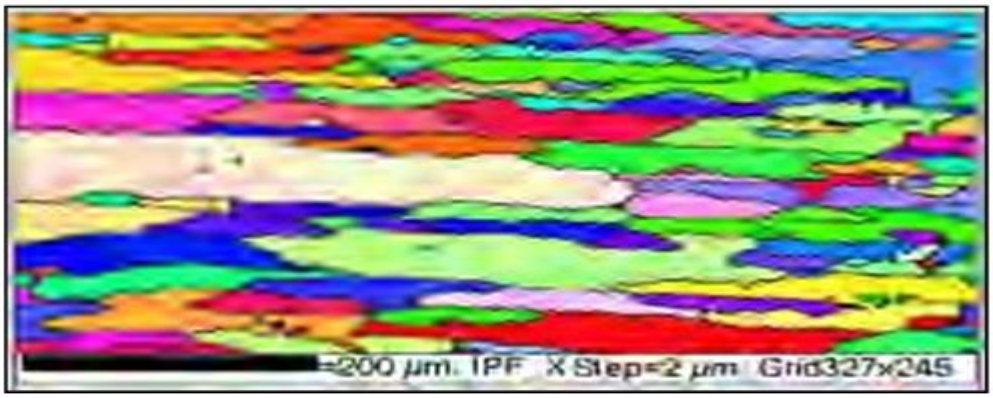

Figure 13. EBSD mapping of the 6082-T6 alloy

4.4.1.1 Grain orientation in the alternating bands:

Figure 14 represents a mapping in the form of an inverse pole figure of the banded structure contained in the AS. The coloring indices are on the right of Figure 14 and will be the same for the other EBSD maps. It is noted that the bands with large grains, colored in blue, have a majority orientation (111) while the bands with smaller grains, colored in green, have rather a (101) orientation. We also observe a band with very fine grains colored in light blue reflecting an orientation between (111) and (101). It can be concluded that the alternating bands show both a difference in grain size and grain orientation.

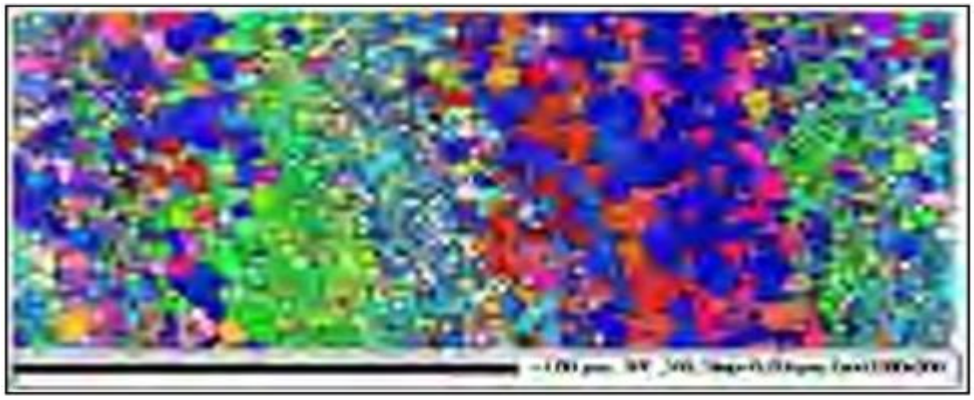

Figure 14. EBSD mapping of the alternating bands corresponding to zone I of Figure 11

4.4.1.2 Grain orientation in the weld center:

Figure 15 shows the EBSD mapping of zones II and III of Figure 12. In zone II, an alternation between two major orientations (111) in blue and (001) in red can be distinguished. While in zone III, the grain color changes to purple and orange with an orientation between (111) and (001). These bands were not visible under the optical microscope which only revealed the "onion rings".

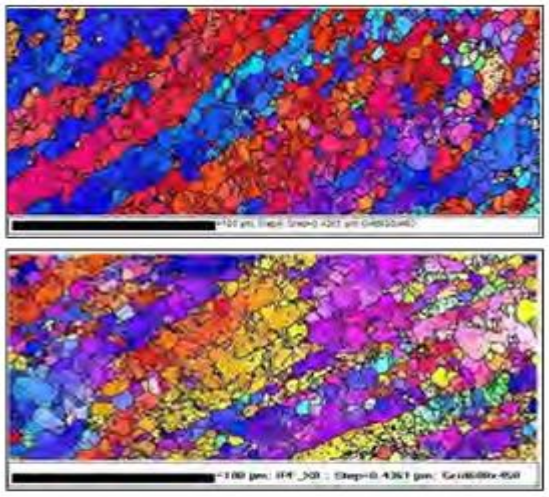

Figure 15. EBSD maps of the tool path area: (a) area corresponding to zone II and (b) zone III of Figure 12

4.4.1.3 Grain orientation in the RS:

Arriving at zone IV in the "retreating" side, we find a more or less homogeneous majority distribution between the (111) and (101) orientations and we only find a few grains colored in red with an orientation (001) as shown in Figure 16.

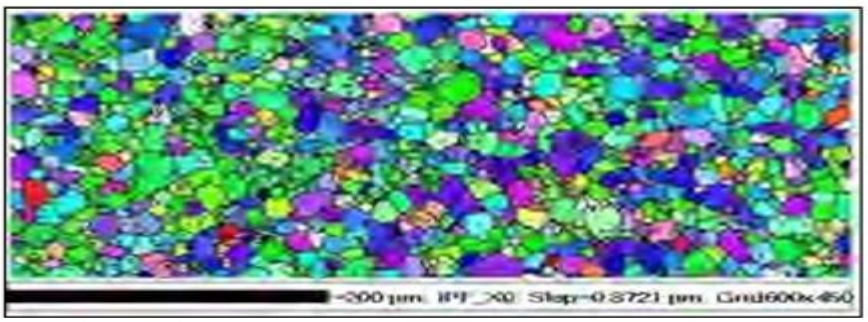

Figure 16. EBSD map of the RS corresponding to zone IV of Figure 12

4.4.2 Grain Disorientation

A post-EBSD analysis was performed on areas I to IV of Figure 12 using the HKL technology of Oxford instruments software.

4.4.2.1 Grain Disorientation in the Base Material

The 6082-T6 AA, which constitutes the base material, is characterized by a very low grain disorientation expressed by a high percentage of about 89% of LA grain boundaries (< 10°). The EBSD map of the base alloy is shown in Figure 17. The green lines represent grain boundaries with an orientation angle between 2° and 10°, the black lines greater than 10° and the red lines greater than 50°. This color code will be used for the EBSD maps that will follow.

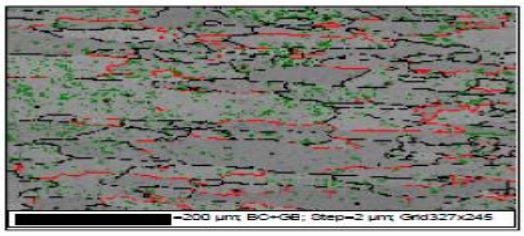

Figure 17. EBSD mapping of the 6082-T6 alloy and the color code of the grain boundary angles

4.4.2.2 Grain misorientation in the alternating bands

Having verified that there is a difference in orientation between the different bands, but also according to the position in the weld, we will now study more closely the grain boundaries and the degree of orientation between them. An EBSD mapping was made for a larger area containing alternating bands (and also containing the indentations of the nano-hardness test). After the chemical attack, an alternation between "dark" bands formed by small grains and "light" bands formed by larger grains was observed with the optical microscope. This alternation is found in the EBSD mapping of Figure 18 (a). But if we look closely at the grain boundaries, we notice that the large grains, which form the "light" bands, are made up of small grains with low angle grain boundaries (LAGBs), < 10° and colored green in Figure 18 (b), which were not visible under the optical microscope. The "dark" bands are mainly made up of grains with high angle grain boundaries (HAGBs) greater than 10° and colored black in Figure 18 (b). The boundaries of the large grains actually have an angle greater than 50° (colored red in the same figure) which are reminiscent of the grain boundaries in the tool path area (colored red in Figures 19 and 20). Figure 19 shows an EBSD map of a small area in a coarse-grained band in (a) where HA boundaries are found enclosing grains with LA boundaries (< 10° in green) and another fine-grained band in (b) with higher-angle boundaries (greater than 10° in black and red).

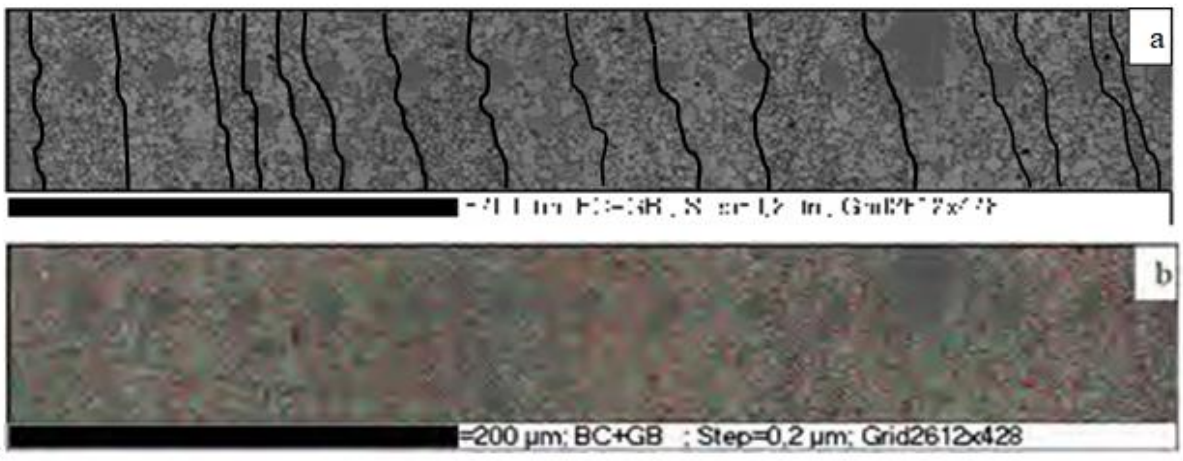

Figure 18. EBSD mapping of alternating bands: (a) alternating between coarse-grained bands and finer-grained bands and (b) Line 1 of Figure 3.9 with grain boundaries and corresponding colour code

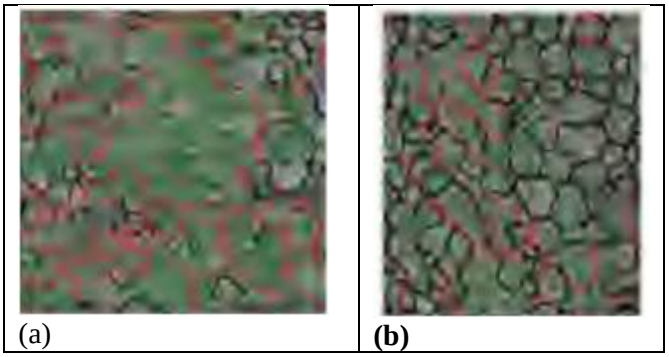

Figure 19. EBSD mapping (a) area of a coarse-grained band and (b) area of a fine-grained band

4.4.2.3 Grain misorientation in the weld centre:

Zones II and III of Figure 15 are characterised by grains grouped in bands of the same orientation. Looking at the grain boundaries, one can recognise the initial grain outline of the parent material but also the formation of small grains inside with LA boundaries. About 87% of the grain boundaries have an angle < 10° (shown in green in Figures 20 and 21) compared to only 13% greater than 10° (shown in black and red). The grain boundaries colored in red have an angle greater than 50°. These values are almost identical for both zones.

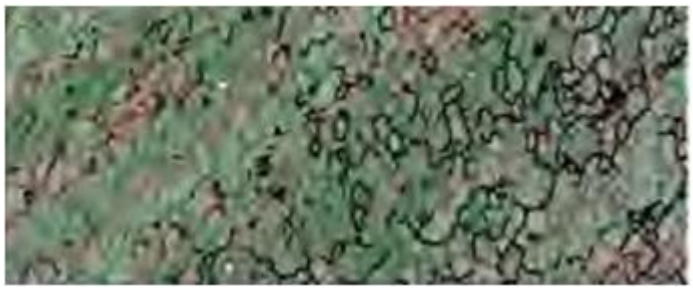

Figure 20. EBSD mapping of zone II on the tool path

Figure 21. EBSD mapping of zone III on the tool path

4.4.2.4 Grain misorientation in the RS

Figure 22 shows a mapping of a post-EBSD analysis of the RS corresponding to zone IV in Figure 12. Equiaxed grains are found with more HA boundaries. The percentage of joints with an angle < 10° is decreased to 74% and that of joints with an angle greater than 10° has doubled (26%) compared to the weld center.

Figure 22. EBSD mapping of zone IV in the RS

4.4.3 Discussion on grain orientation and misorientation

FSW has always been divided into four distinct zones (BM, HAZ, TMAZ and SZ). However, the stirred zone or (stir zone SZ) undergoes complex phenomena of deformation and temperature leading to a heterogeneous microstructure. The study of grain orientation in the microstructure is one of the means that has helped researchers understand the mechanism of deformation and material flow that occur in FSWs. Several have been interested in this zone but given the different cases, the data remains insufficient. Indeed, the WP (rotation and feed speeds as well as the tool used) lead to different structures. If a tool containing threads is used, the movement of the material will be better favored and a different microstructure would be obtained. We have seen that this orientation is not homogeneous in the core. We have distinguished three zones which themselves present heterogeneities. The center of the core is the area where the tool begins to tear off material and thanks to the elongated shape of the grains, the trajectory of the material can be followed. The RS, consisting of equiaxed grains with random orientation, is evidence of dynamic recrystallization. The AS, for its part, consists of an alternation between a band of material that can come from the RS and another from the center of the weld. This alternation that forms the alternating bands is a combination of difference in size and grain orientation.

A research on a dissimilar weld between the AA 6061-T6 and the alloy 5052-O, shows a homogeneous stirred zone on both sides (AS) and (RS) with the absence of LAGB reflecting the complete recrystallization of the grains [7]. Yadav and Bauri found that in friction stir welding (FSW) of 99.2% pure commercial aluminum, the weld center had a preferred orientation (001) with a lower percentage of HAGB compared to the advancing (AS) and receding (RS) sides which had a random grain orientation [22]. An explanation for this difference in the degrees of orientation has been explained by Prangnell and Heason. The material along the tool path undergoes a gradual increase in temperature and strain rate and the base material grains start to split into large grains that form bands as seen in Figures 20 and 21. These grains appear larger because they contain small grains with very low angle boundaries. This is the beginning of recrystallization. As strain increases, subgrains are formed by the movement of dislocations that arrange themselves in the boundaries. This results in grains with LA grain boundaries (LAGB). These LA grain boundaries (LAGB) transform into HA grain boundaries (HAGB) during continuous dynamic recrystallization ([23]; [22]). This trend is seen in the RS of our weld (Figure 22) where the percentage of grains with HA grain boundaries has increased. Using EBSD analysis, it was possible to see that the alternation between light and dark bands observed under the optical microscope was due to a difference in their response to chemical attack as they underwent different strain rates and temperature histories. According to the Hall-Petch principle, the small grain size in the dark bands should increase the hardness compared to the light bands [22]. However, in our study, no significant difference in the hardness of the bands was observed except for points 5 and 6 where the "finer" grained band has a higher hardness than the "coarser" grained one. Points 14 and 15 show an inverse behavior and this suggests that other factors could condition the hardness. The HA grain boundaries and the LA subgrain boundaries formed by the absorption of dislocations could be the cause since the alternating bands would have different dislocation densities. Researchers have stipulated that it is rather the Orowan mechanism that dominates during the friction-stir process [24]. By this principle, the size of the precipitates influences the movement of the dislocations and consequently the hardness of the material. This leads us, in the following, to study the distribution of the precipitates in different areas of the weld nugget.

4.5 Analysis of the distribution of precipitates

An energy dispersive analysis (EDS) was carried out on the base material and the four different zones of Figure 12. In the banded structure, the bands where the decrease in hardness was noted were chosen.

4.5.1 Precipitates in the base material, weld center and RS

4.5.1.1 Mg-Si precipitates

In the base material, the magnesium distribution is homogeneous and there are several silicon particles. When looking at the tool path area in the middle of the weld (zone II and III of Figure 12), the dissolution of magnesium and silicon is observed. On the other hand, an agglomeration of these components is observed in the RS (zone IV of Figure 12) as in Tabl

Table 4. Distribution of silicon and magnesium in the base material, weld center and RS

	EDS Si	EDS Mg	EDS Si-Mg
Base Material	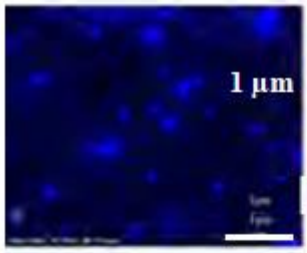	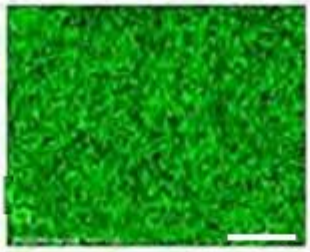	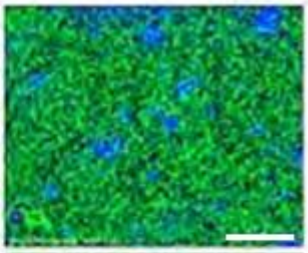
Zone II Weld Center	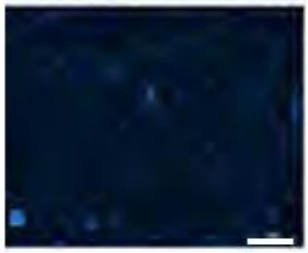	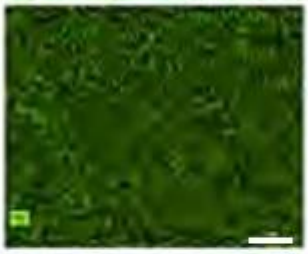	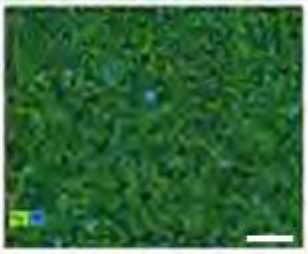
Zone III Weld Center	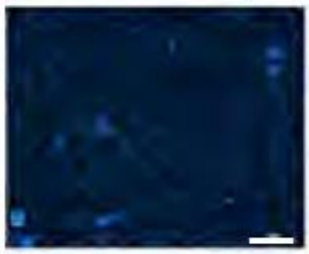	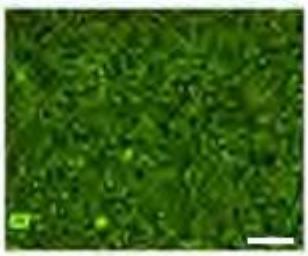	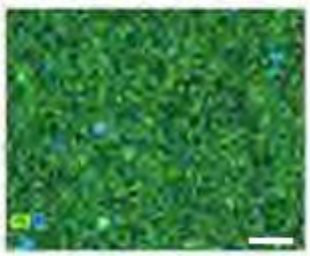
RS	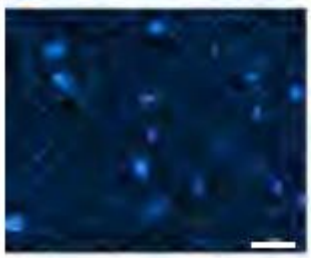	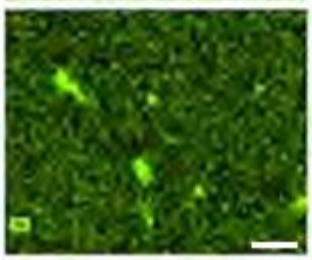	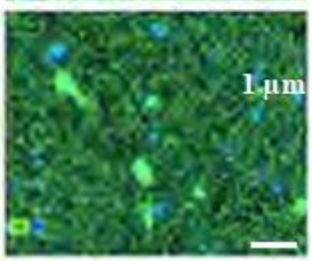

4.5.1.2 Mn-Si precipitates

Since manganese is one of the main components of 6061 and 6082 AAs, EDS analysis allowed us to see its presence in the different zones of the weld. Table 5 shows the distribution of manganese in the base material, in the middle of the weld on the tool path (zone II and III of Figure 12) and in the RS (zone IV of Figure 12). The manganese present in the base material is almost dissolved in the weld and in particular on the tool path.

Table 5. Distribution of silicon and manganese in the base material, weld center and RS

	EDS Si	EDS Mn	EDS Si-Mn
Base Material	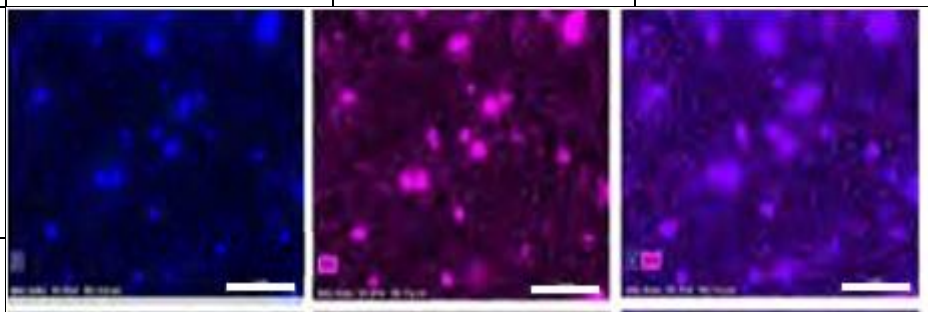		
Weld Center Zone II	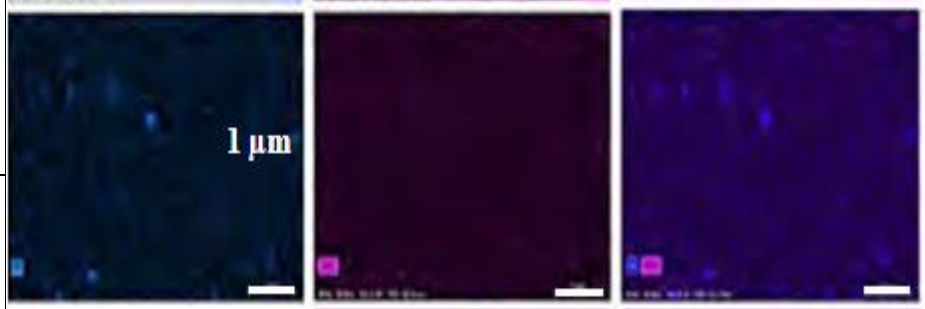		
Weld Center Zone III			
Retreat Side	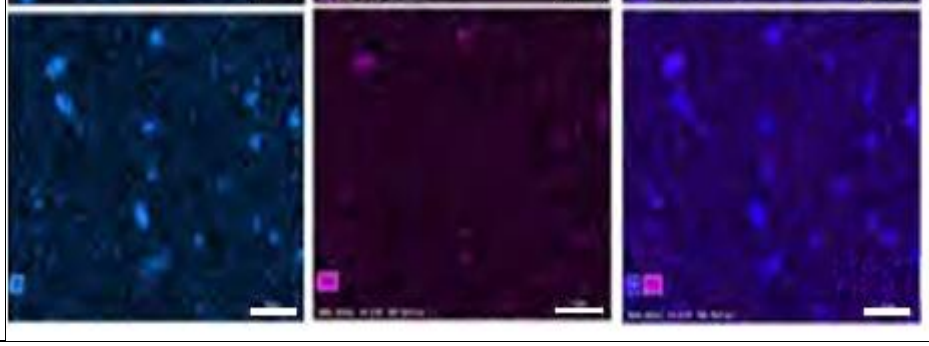		

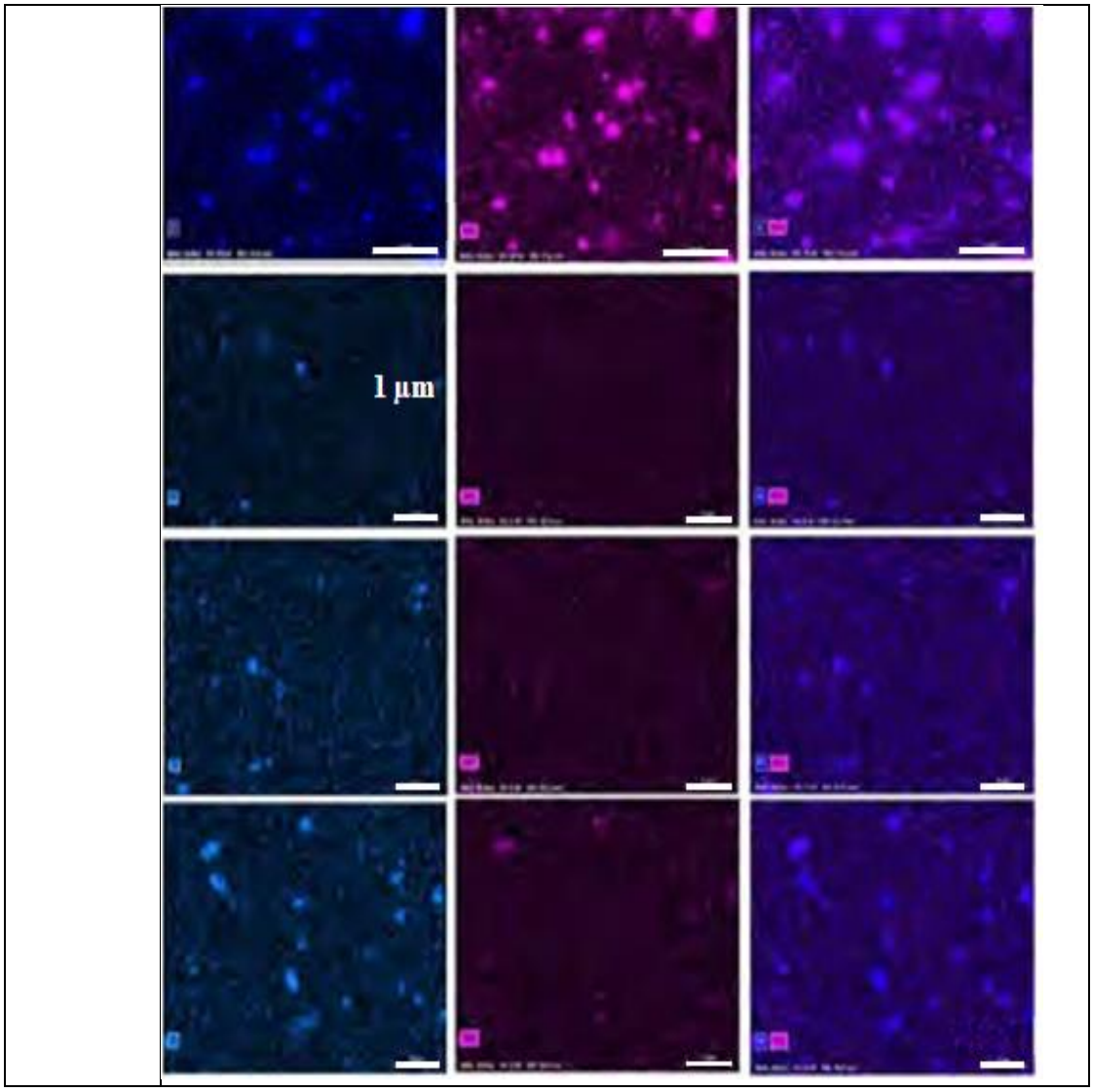

4.5.2 Precipitates in alternating bands

EDS analysis was done on the bands containing indentations 5, 6 of lines 1 and 2 where a decrease in hardness was observed in Figure 10. The band containing indentation 5 is formed by finer grains with HA joints than the one containing indentation 6. The hardness is higher in the first band and this can be explained by a higher concentration of precipitates as can be observed in Figure 23. Magnesium and silicon are observed but not much Mg2Si precipitates. During FSW, heat-treated alloys lose their T6 property by the dissolution of very fine hardening precipitates and the coarsening of non-hardening precipitates [25]. The coarsening of iron, silicon and manganese precipitates is also noted in Figure 24.

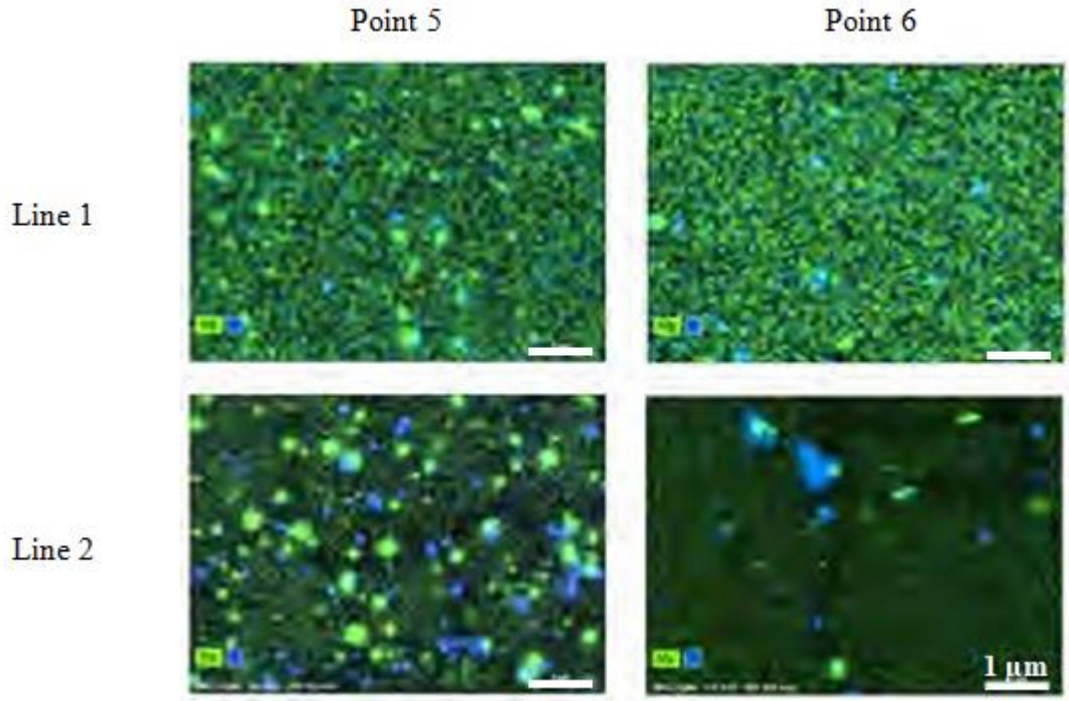

Figure 23. Distribution of silicon and magnesium in the fine-grained band (point 5 of lines 1 and 2) and the coarse-grained band (point 6 of lines 1 and 2)

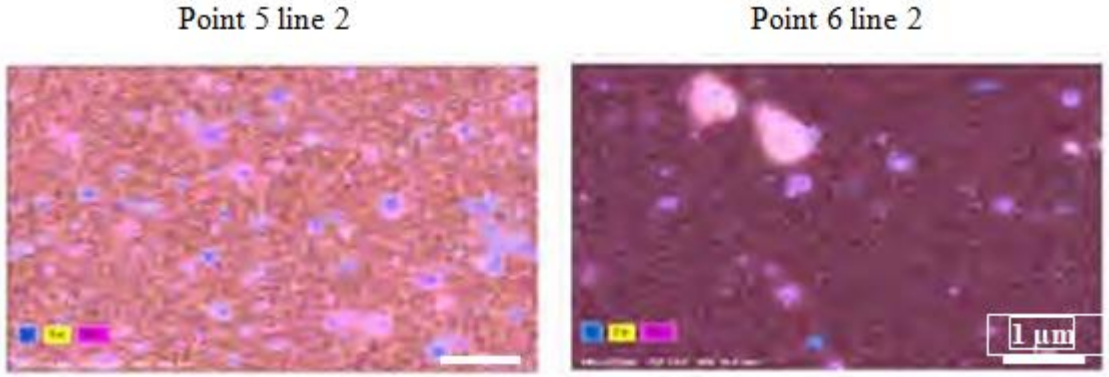

Figure 24. Distribution of silicon, iron and manganese in the fine-grained band (point 5 of line 2) and the coarse-grained band (point 6 of line 2)

4.5.3 Discussion on precipitation

The MP of the weld of hardening alloys are conditioned by the distribution of the precipitates, with the grain size having a lesser effect. It was observed that the precipitates present in the base material were dissolved on the tool path (area containing grains with LA boundaries) because this area undergoes the highest temperature, which implies a slower cooling time that does not allow the alloying elements to be maintained in the matrix. The precipitates found on the RS (containing grains with HA boundaries) could be due to slower cooling.

In a study of a 6061-T6 alloy, Sauvage et al. found that the weld core was free of β" precipitates but that magnesium and silicon dispersoids were still present. They also noted that their distribution was heterogeneous and that they agglomerated in certain areas. They explained that some precipitates resisted the high temperature and then grew during cooling [26]. J.F Guo explained, during a study of a dissimilar weld between AA6061 and AA 7075, that the decrease in hardness in the HAZ is due to the disappearance of the Guinier-Preston (G.P) zones and the enlargement of the hardening precipitates and compared this phenomenon to aging while in the ZATM this process is accentuated comparing it to

solution treatment. On the other hand, reprecipitation is possible in the core which reaches higher temperatures [27]. They agree with Sauvage et al., in noting that with the temperature increase in the core reaching 0.8 Tf, i.e. exceeding 400°C, the hardening precipitates β" characteristic of the 6000 series, stable at a temperature below 200°C, dissolve. This high temperature allows the coarsening of β' precipitates which have a less significant hardening effect than β" [28]. Lee et al. stipulate that the cooling rate would be fast enough to maintain the alloying elements in a saturated solid solution [29].

In the AS and more precisely in the "onion rings", the precipitates are distributed heterogeneously. The very fine grain bands (grains with high angle boundaries) contain more magnesium, silicon and iron than the coarse grain bands (grains with low angle boundaries) as can be seen in the fine grain band containing points 5 of lines 1 and 2 in Figure 23 which contains more particles compared to the band containing points 6 of lines 1 and 2. Mahoney et al. had also observed, in a weld of a 7075-T651 alloy, that the bands with Fine grains contained chromium dispersoids and $MgZn_2$ precipitates while coarse grained bands contained less [30]. This alternation could be due to the rotation and feed of the tool which deposits successive layers of material coming sometimes from the RS (with recrystallized grains) and sometimes from the center of the core (with partially recrystallized grains). It has been reported by several researchers that the weld core as well as the heat affected zone can undergo the complete dissolution of the precipitates or their coarsening depending on the temperature cycles undergone by the material themselves depending on the rotation and feed speeds. ([31]; [32]). Svenson et al., in a study of dissimilar welds of alloys 5083 and 6082, did not observe any particular difference in grain size or precipitate density between the alternating bands but found that very fine hardening precipitates < 10 nm were completely dissolved in the core and that the density of the 6082 precipitates of 0.1 to 1 µm and 1 to 10 µm had increased, concluding that this is a coarsening of the precipitates [33]. In the 6082 core, they found large precipitates of 1 to 5 µm which they identified as AlFe(Mn)Si or β (Mg2Si) and finer Al-Mn-Si particles of 100 to 150 nm. The very localized difference in hardness and therefore in the distribution of β' and β precipitates in the core would depend on the temperature reached, the holding time at high temperature and the cooling rate. The presence of these particles retards grain growth, which can be demonstrated by the EDS presented previously. Researchers were unanimous on the dissolution of hardening precipitates in the welds of 6000 series alloys, but it is still preferable to check their presence as well as the density of dislocations with transmission electron microscopy, which was not done due to lack of time.

Finally, this part allowed us to confirm that within the core there is a heterogeneity in the distribution of precipitates reflecting a different thermal and mechanical history.

In the next part, it will be a question of studying the MP to correlate them with the observations of the microstructure.

5. CONCLUSION:

Very complex phenomena occur during FSW. The feed and RSs but also the tool used condition the temperature cycles depending on the alloy used which in turn determine the microstructure of the weld and its MP. The analysis of FSWs led to the following conclusions:

- The alternating bands depend on the WP as well as the geometry of the tool and can appear even in so-called "hot" welds by increasing the RS.
- The alternating bands appear as a contrast difference observed under an optical microscope. They are due, at first glance, to a difference in grain size. It turned out that this difference is due to an alternation between bands containing grains with LA boundaries of predominant orientation (101) and others with HA orientation (111).
- Hardness tests (Vikers and nano-indentation) did not reveal a difference in hardness between the alternating bands.
- The center of the weld core is formed by large grains with high angle joints containing smaller grains with low angle joints. These grains could be the origin of the coarse grains contained in the light bands.

- The RS is formed by equiaxed grains with high angle joints with random orientation. These grains could be the origin of the very fine grains contained in the dark bands.
- The areas formed by grains with high angle joints (RS and dark bands) are richer in particles than those formed by grains with low angle joints (center of the weld and light bands)

REFERENCES:

1. Hamilton, C. H., Dymek, S., & Blicharski, M. (2010). Precipitation strengthening in friction stir welds of 6XXX series aluminum alloys. Materials Science and Technology, 26(10), 1145-1151.
2. Krishnan, K. N. (2002). On the formation of onion rings in friction stir welds. Materials Science and Engineering: A, 327(2), 246-251.
3. Mahoney, M. W., Rhodes, C. G., Flintoff, J. G., Bingel, W. H., & Spurling, R. A. (2008). Properties of friction-stir-welded 7075 T651 aluminum. Metallurgical and Materials Transactions A, 29(7), 1955-1964.
4. Mishra, R. S., & Ma, Z. Y. (2005). Friction stir welding and processing. Materials Science and Engineering: R: Reports, 50(1-2), 1-78.
5. Prater, T., Burek, M., Putt, C. W., Walker, L., & Santos, R. (2019). Microstructural evolution and mechanical properties of 6061-T6 aluminum friction stir welded joints. Journal of Materials Processing Technology, 271, 168-178.
6. Su, H., Wu, C. S., & Huang, Y. X. (2019). Recent development and applications of friction stir welding: A review. Materials & Design, 182, 108007.
7. Wang, Y., Zhang, H., & Zuo, H. (2023). Effect of friction stir welding parameters on the microstructure and mechanical properties of 6061 aluminum alloy. Journal of Manufacturing Processes, 81, 1100-1111. https://doi.org/10.1016/j.jmapro.2022.12.037
8. Prater, T., Burek, M., Putt, C. W., & Santos, R. (2022). Impact of welding parameters on the grain structure and mechanical properties of friction stir welded 6061-T6 aluminum alloy. Materials Science and Engineering: A, 853, 143921. https://doi.org/10.1016/j.msea.2022.143921
9. Su, H., Wu, C. S., & Huang, Y. X. (2019). Advances in friction stir welding of aluminum alloys: Process parameters, microstructure, and mechanical properties. Materials Science and Engineering: A, 758, 56-68. https://doi.org/10.1016/j.msea.2019.04.089
10. Gharacheh, M., Mohammadi, J., Amirkhanlou, S., & Bostanabad, R. (2020). Effect of process parameters on the microstructure and mechanical properties of friction stir welded 7075 aluminum alloy. Metallurgical and Materials Transactions A, 51(12), 6202-6215. https://doi.org/10.1007/s11661-020-06016-8
11. Kumar, R., Kaushik, N., & Mishra, V. K. (2021). Analysis of grain boundary bands in friction stir welded aluminum alloys: Influence of tool geometry and process parameters. Journal of Materials Research and Technology, 11, 1105-1114. https://doi.org/10.1016/j.jmrt.2020.12.105
12. Bai, Y., & Zhang, Y. (2021). Dynamic recrystallization mechanisms in friction stir welded 6082-T6 aluminum alloy. Acta Materialia, 212, 116897. https://doi.org/10.1016/j.actamat.2021.116897
13. Mishra, R. S., & Ma, Z. Y. (2022). Recent developments in friction stir welding and processing of high-strength aluminum alloys. Progress in Materials Science, 124, 100844. https://doi.org/10.1016/j.pmatsci.2021.100844
14. Patil, S., Dixit, U., & Mubeen, S. (2022). Effect of cooling media on microstructure and properties of friction stir welded aluminum alloys. Materials Today: Proceedings, 56, 3451-3458. https://doi.org/10.1016/j.matpr.2022.03.123
15. Wang, J., Zhang, D., & Li, Y. (2023). Hybrid friction stir welding using advanced tool materials for improved weld quality in aluminum alloys. Journal of Manufacturing Science and Engineering, 145(4), 041011. https://doi.org/10.1115/1.4055068
16. Sharma, S., Dwivedi, D., & Kumar, S. (2012). Investigation of the effect of process parameters on the mechanical properties of friction stir welded 6061 aluminum alloy. Journal of Materials Processing Technology, 212(10), 2143-2154. https://doi.org/10.1016/j.jmatprotec.2012.04.019
17. Schneider, M., & Nunes, A. (2004). Investigation of the effects of process parameters on the microstructure and mechanical properties of friction stir welds in aluminum alloys. Science and Technology of Welding and Joining, 9(4), 263-268. https://doi.org/10.1179/136217104225021617

18. Sutton, M. A., Caster, J. D., & Fiedler, D. (2002). Investigation of microstructure and mechanical properties of friction stir welds in high-strength aluminum alloys. Materials Science and Engineering: A, 325(1-2), 150-160. https://doi.org/10.1016/S0921-5093(01)01581-3

19. Lim, J. H., Lee, C. S., & Kim, Y. J. (2004). Microstructure and mechanical properties of friction stir welded 6061 aluminum alloy. Materials Science and Engineering: A, 370(1-2), 295-302. https://doi.org/10.1016/j.msea.2003.09.020

20. Rajakumar, S., Muralidharan, C., & Balasubramanian, V. (2011). Influence of friction stir welding process parameters on the mechanical properties of aluminum alloy joints. Materials and Design, 32(4), 2316-2325. https://doi.org/10.1016/j.matdes.2010.11.029

21. Prisco, U. D., Di, A. A., & Beatrice, C. (2013). Friction stir welding of aluminum alloys: Influence of tool design and process parameters on joint performance. Materials Science and Engineering: A, 580, 53-61. https://doi.org/10.1016/j.msea.2013.04.072

22. Yadav, S. K., & Bauri, R. (2012). Effect of process parameters on microstructure and mechanical properties of friction stir welded joints of AA5083 aluminum alloy. Materials and Design, 42, 7-15. https://doi.org/10.1016/j.matdes.2012.05.011

23. Prangnell, P. B., & Heason, P. (2005). The influence of process parameters on the mechanical properties and microstructure of friction stir welded 6000 series aluminium alloys. Materials Science and Technology, 21(8), 1-11. https://doi.org/10.1179/174328405X45295

24. Sato, Y., Park, H. S., & Kokawa, H. (2001). Microstructural evolution in friction stir welded 6061 aluminum. Scripta Materialia, 44(5), 665-669. https://doi.org/10.1016/S1359-6462(00)00496-0

25. Çam, E., & Mistikoglu, G. (2014). Effect of tool geometry on the friction stir welding of AA6061 aluminum alloy. Journal of Materials Processing Technology, 214(10), 2079-2086. https://doi.org/10.1016/j.jmatprotec.2014.05.017

26. Sauvage, X., Tingaud, D., & Reider, P. (2008). The influence of the microstructure and texture of the weld zone on the mechanical properties of friction stir welds. Materials Science and Engineering: A, 481-482, 328-333. https://doi.org/10.1016/j.msea.2007.04.104

27. Guo, Y. B., Ma, Z. Y., & Li, L. (2014). Microstructure and mechanical properties of friction stir welded joints of AA7050-T6 aluminum alloy. Journal of Materials Processing Technology, 214(4), 746-754. https://doi.org/10.1016/j.jmatprotec.2013.12.011

28. Svensson, L. E., Selander, S., & Andersson, G. (2000). Microstructural investigations of friction stir welding of aluminum alloys. Materials Science and Engineering: A, 287(2), 282-289. https://doi.org/10.1016/S0921-5093(00)01083-8

29. Lee, S. H., Yeon, H. J., & Jung, Y. G. (2003). Microstructural evolution and mechanical properties of friction stir welded aluminum alloys. Materials Science and Engineering: A, 355(1-2), 237-245. https://doi.org/10.1016/S0921-5093(03)00324-6

30. Mahoney, M. W., Barnes, S. S., & Wright, S. I. (1998). Microstructural evolution in friction stir welding of high-strength aluminum alloys. Scripta Materialia, 39(1), 47-53. https://doi.org/10.1016/S1359-6462(98)00123-5

31. Tang, W., Zhang, J., & Li, Z. (1998). The effect of friction stir welding on the microstructure and mechanical properties of 7xxx aluminum alloys. Materials Science and Engineering A, 253(1-2), 62-69. https://doi.org/10.1016/S0921-5093(98)00358-5

32. Moreira, P. M. G., Pinto, A. A. M., & Ferreira, J. M. (2009). A comprehensive study of the friction stir welding process in aluminum alloys. Journal of Materials Processing Technology, 209(3), 1833-1842. https://doi.org/10.1016/j.jmatprotec.2008.03.010

33. Svensson, L., Larsson, R., & Isberg, J. (2000). Friction stir welding of high strength aluminum alloys. Journal of Materials Processing Technology, 103(1-3), 142-148. https://doi.org/10.1016/S0924-0136(00)00752-0